Optics and Lasers in Engineering 91 (2017) 232–241

Contents lists available at ScienceDirect

Optics and Lasers in Engineering

journal homepage: www.elsevier.com/locate/optlaseng

Pixel-by-pixel absolute phase retrieval using three phase-shifted fringe patterns without markers

Chufan Jiang, Beiwen Li, Song Zhang*

School of Mechanical Engineering, Purdue University, West Lafayette, Indiana 47907, USA

ARTICLE INFO

Keywords:
Absolute phase
Real-time
Structured light
Geometric constraints
Depth range extension

ABSTRACT

This paper presents a method that can recover absolute phase pixel by pixel without embedding markers on three phase-shifted fringe patterns, acquiring additional images, or introducing additional hardware component(s). The proposed three-dimensional (3D) absolute shape measurement technique includes the following major steps: (1) segment the measured object into different regions using rough priori knowledge of surface geometry; (2) artificially create phase maps at different z planes using geometric constraints of structured light system; (3) unwrap the phase pixel by pixel for each region by properly referring to the artificially created phase map; and (4) merge unwrapped phases from all regions into a complete absolute phase map for 3D reconstruction. We demonstrate that conventional three-step phase-shifted fringe patterns can be used to create absolute phase map pixel by pixel even for large depth range objects. We have successfully implemented our proposed computational framework to achieve absolute 3D shape measurement at 40 Hz.

1. Introduction

Three-dimensional (3D) shape measurement has been adopted in many applications including but not limited to online inspection in manufacturing and disease diagnosis in medicine.

To achieve high-quality 3D shape measurements, typically, phase-based techniques have advantages over intensity-based techniques because of their merits of high spatial resolutions and robustness to noise or surface reflectivity variations. A variety of phase analysis techniques have been developed over the years including the Fourier transform method [1], the Windowed Fourier transform method [2,3] and the phase-shifting methods [4]. In general, a phase analysis technique only produces wrapped phase maps ranging from $-\pi$ to π with 2π discontinuities, and thus a phase unwrapping algorithm is necessary to generate continuous phase maps without 2π discontinuities.

Existing phase unwrapping approaches can be classified into three major categories: spatial phase unwrapping, temporal phase unwrapping, and phase unwrapping by adding additional hardware components (e.g., a camera). A spatial phase unwrapping algorithm basically locates 2π discontinuities by inspecting surrounding pixels on the phase map itself and removes them by adding or subtracting integer number $k(x, y)$ of 2π. Such integer number $k(x, y)$ is often referred as *fringe order*. Numerous spatial phase unwrapping methods have been summarized in the book [5] and by Su and Chen [6]. Yet the spatial phase unwrapping has two fundamental limitations: (1) only produces a continuous phase map that is *relative* to the phase value of a pixel within a smoothly connected component, and thus the unwrapped phase map is a *relative* phase map; and (2) could fail if there exists spatially isolated objects or surfaces with abrupt geometric discontinuities. To produce an *absolute* phase map from spatial phase unwrapping, researchers have come up with ideas that embed markers into a single fringe pattern [7–9] or several phase-shifted patterns [10–12] to adjust relative fringe order $k(x, y)$ to be absolute ones. Though working, these marker embedded methods could encounter problems if the embedded marker is not visible on the captured region of interest.

A temporal phase unwrapping method determines fringe order $k(x, y)$ by acquiring additional information. Fringe order is determined by looking for pre-defined cues of the same pixel from those additional images. Since those cues can be pre-defined, the fringe order determined from these methods is *absolute* and the unwrapped phase is absolute phase. Over the years, researchers have come up with a variety of temporal phase unwrapping methods including multi-frequency (or -wavelength) phase-shifting methods [13–16], binary coding methods [17,18], phase coding methods [19–21], etc. All these existing temporal phase unwrapping algorithms can work well in retrieving absolute phase map. However, temporal phase unwrapping approaches sacrifice measurement speed by requiring additional image acquisition, making them undesirable for high-speed applications.

To address the limitation of reduced measurement speed for

* Corresponding author.
E-mail address: szhang15@purdue.edu (S. Zhang).

http://dx.doi.org/10.1016/j.optlaseng.2016.12.002
Received 6 September 2016; Received in revised form 3 November 2016; Accepted 2 December 2016

conventional temporal phase unwrapping approaches, researchers proposed to add the second camera [22–26]. The idea lies in the fact that the wrapped phase value should appear the same in both cameras, and thus only limited number of candidates are available if combining the epipolar geometry with stereo vision. Yet the approaches proposed in [22–25] require global backward and forward searching to select the correct point out of all candidate points, which results in slow computational speed. Although Lohry and Zhang [26] proposed to speed up the correspondence detection by embedding statistical patterns into original fringe patterns, the correspondence refinement process is still very slow. Overall, adding a second camera increases system design complexity and cost, which is not desirable for practical applications; and also increases shadow/occlusion areas since a point has to been "seen" by the third perspective in order to be measurement.

To overcome the limitations of all existing absolute phase recovery approaches, An et al. [27] recently proposed a pixel-wise phase unwrapping method by solely using geometric constraints of structured light system without capturing additional images, or adding another camera. The basic idea is to generate an artificial absolute phase map Φ_{min} from a virtual depth plane z_{min} for absolute phase unwrapping, which will be detailed in Section 2.3. However, as mentioned by An et al. [27], the fundamental limitation of this approach is its confined depth sensing range.

This paper presents a novel phase unwrapping framework to substantially increase depth range of the phase unwrapping method developed by An et al. [27]. Instead of using one single Φ_{min}, we propose to create additional Φ_{min} at different virtual planes. We utilize rough prior-knowledge of the surface geometry information to segment the image into different depth regions and select a proper Φ_{min} map for each region to achieve pixel by pixel phase unwrapping. The overall unwrapped phase is then generated by combining those unwrapped phase maps of different regions. We have developed a hardware system to verify the performance of this proposed computational framework. Our experiments demonstrated that we can achieve absolute 3D shape measurement at 40 Hz with only three phase-shifted fringe patterns for a rather large depth range.

Section 2 introduces the related principles and our proposed computational framework; Section 3 demonstrates the experimental validations and real-time 3D shape measurements realizations of our proposed framework; and Section 4 summarizes our proposed research work.

2. Principles

2.1. Three-step phase shifting algorithm

Phase-shifting algorithms are extensively used in optical metrology because of their high accuracy and robustness. Numerous phase-shifting algorithms have been developed with different requirements on the number of fringe patterns and phase shifts between fringe patterns. Among all phase-shifting algorithms, the three-step phase-shifting algorithm has the advantage of requiring the minimum number of patterns for phase recovery, which is preferable for high-speed measurements. Three phase-shifted fringe patterns with equal phase shifts can be mathematically described as:

$$I_1(x, y) = I'(x, y) + I''(x, y)\cos[\phi - 2\pi/3], \tag{1}$$

$$I_2(x, y) = I'(x, y) + I''(x, y)\cos[\phi], \tag{2}$$

$$I_3(x, y) = I'(x, y) + I''(x, y)\cos[\phi + 2\pi/3], \tag{3}$$

where $I'(x, y)$ is the average intensity, $I''(x, y)$ is the intensity modulation, and ϕ is the phase to be solved for. Simultaneously solving the above three equations leads to

$$\phi(x, y) = \tan^{-1}\left[\frac{\sqrt{3}\,(I_1 - I_3)}{2I_2 - I_1 - I_3}\right]. \tag{4}$$

Because the phase is obtained from an arctangent function, it is wrapped ranging from $-\pi$ to π with 2π discontinuities. A phase unwrapping algorithm is required for removing 2π discontinuities to obtain a continuous phase map. Different from conventional spatial or temporal phase unwrapping methods, the following few sections introduce the newly proposed phase unwrapping algorithm using geometric constraints [27] without capturing any additional images.

2.2. Digital fringe projection (DFP) system model

We first discuss DFP system model since it is the key to understand how geometric constraints can be used to retrieve absolute phase. The imaging lenses (e.g. camera lens, projector lens) in the DFP system follow the well-known pinhole model [28]. This linear pinhole model essentially formulates the projection from 3D world coordinate (x^w, y^w, z^w) to 2D imaging coordinate (u,v), which can be mathematically represented by the following equation:

$$s\begin{bmatrix} u \\ v \\ 1 \end{bmatrix} = \begin{bmatrix} f_u & \gamma & u_0 \\ 0 & f_v & v_0 \\ 0 & 0 & 1 \end{bmatrix}\begin{bmatrix} r_{11} & r_{12} & r_{13} & t_1 \\ r_{21} & r_{22} & r_{23} & t_2 \\ r_{31} & r_{32} & r_{33} & t_3 \end{bmatrix}\begin{bmatrix} x^w \\ y^w \\ z^w \\ 1 \end{bmatrix}, \tag{5}$$

where s is the scaling factor; f_u and f_v are effective focal lengths of the imaging lens along u and v directions; γ is the skew factor of u and v axes; (u_0, v_0) is the principle point; r_{ij} and t_i represent the rotation and translation parameters respectively. To further simplify the expression, we define a projection matrix $\mathbf{P}$ as:

$$\mathbf{P} = \begin{bmatrix} f_u & \gamma & u_0 \\ 0 & f_v & v_0 \\ 0 & 0 & 1 \end{bmatrix}\begin{bmatrix} r_{11} & r_{12} & r_{13} & t_1 \\ r_{21} & r_{22} & r_{23} & t_2 \\ r_{31} & r_{32} & r_{33} & t_3 \end{bmatrix} = \begin{bmatrix} p_{11} & p_{12} & p_{13} & p_{14} \\ p_{21} & p_{22} & p_{23} & p_{24} \\ p_{31} & p_{32} & p_{33} & p_{34} \end{bmatrix}. \tag{6}$$

The projection matrix $\mathbf{P}$ can be estimated by well-developed camera calibration toolboxes.

Consider the mutually inverted optics of the camera and the projector [29], same pinhole model is also applicable to the projector. If we perform the calibration for the camera and the projector under the same world coordinate (x^w, y^w, z^w), we can physically correlate two sets of equations from the camera and the projector lenses:

$$s^c[u^c \;\; v^c \;\; 1]^t = \mathbf{P^c}[x^w \;\; y^w \;\; z^w \;\; 1]^t, \tag{7}$$

$$s^p[u^p \;\; v^p \;\; 1]^t = \mathbf{P^p}[x^w \;\; y^w \;\; z^w \;\; 1]^t. \tag{8}$$

Here, superscript ^{p} represents the projector, superscript ^{c} represents the camera, and ^{t} indicates matrix transpose.

Eqs. (7)–(8) above only provide 6 equations with 7 unknowns, s^c, s^p, x^w, y^w, z^w, u^p and v^p, which requires one additional equation to solve 3D coordinates (x^w, y^w, z^w) uniquely. The additional equation can be provided by the linear relationship between phase Φ and a projector pixel line u^p,

$$u^p = \Phi \times T/(2\pi). \tag{9}$$

assuming fringe stripes remain constant along v^p direction or vary along u^p direction. Here T is fringe period in pixels, and Φ must be *absolute* phase. However, the phase extracted from phase-shifting algorithm is wrapped ranging from $-\pi$ to π with 2π discontinuities. Existing absolute phase retrieval methods typically require capturing additional images or use embedded markers. In the next section, we will introduce the absolute phase retrieval method proposed by An et al. [27] which does not require any additional images capture or embedded markers.

2.3. Absolute phase retrieval using geometric constraints

An et al. [27] proposed a pixel-by-pixel phase unwrapping algorithm based on the geometric constraints of the DFP system, whose principle will be explained in details. Fig. 1(a) illustrates how geometric constraints can assist in phase unwrapping. If the camera sensor (charge

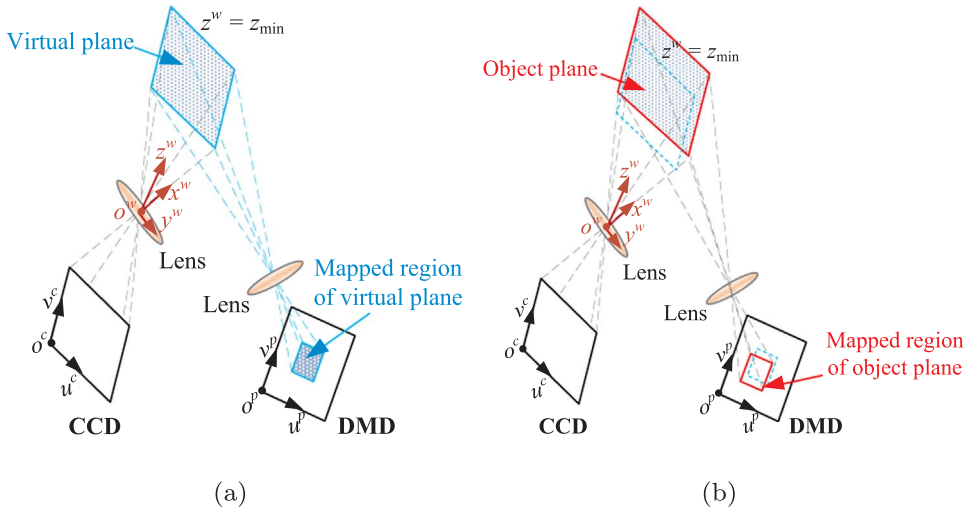

Fig. 1. Mapping between the camera sensor (CCD) and the corresponding region on the projector sensor (DMD) [27]. (a) Mapped projection region for a virtual minimum plane $z = z_{min}$; (b) mapped projection regions for object at z.

coupled device, CCD) captures a region on a flat plane at $z^w = z_{min}$, which is located at the closest depth plane of the entire measurement volume, the same region is mapped to the projector digital-micro-mirror device (DMD) creating a pixel-wise artificial absolute phase map Φ_{min}. This ideally generated artificial absolute phase map Φ_{min} can be used to find where 2π discontinuities are located on a wrapped phase map ϕ, or equivalently, find the fringe order $k(x, y)$. The estimation of z_{min} is of crucial importance to correctly determine the fringe order solely from Φ_{min}. If the real object is placed at distance z that is further way from the system, the mapped region on the projector changes accordingly, as illustrated in Fig. 1(b).

For a calibrated DFP system, all parameters in projection matrices P^c and P^p are determined during calibration process. With a given z_{min}, corresponding x^w and y^w for each camera pixel (u^c, v^c) can be computed by simultaneously solving Eqs. (7) and (8),

$$\begin{bmatrix} x^w \\ y^w \end{bmatrix} = A^{-1}b, \tag{10}$$

where

$$A = \begin{bmatrix} p^c_{31}u^c - p^c_{11} & p^c_{32}u^c - p^c_{12} \\ p^c_{31}v^c - p^c_{21} & p^c_{32}v^c - p^c_{22} \end{bmatrix}, \tag{11}$$

$$b = \begin{bmatrix} p^c_{14} - p^c_{34}u^c - (p^c_{33}u^c - p^c_{13})z_{\min} \\ p^c_{24} - p^c_{34}v^c - (p^c_{33}v^c - p^c_{23})z_{\min} \end{bmatrix}. \tag{12}$$

Here, $p_{ij}{}^c$ indicates the element in the i-th row and j-th column of matrix P^c. Once (x^w, y^w) is obtained, the projector pixel (u^p, v^p) corresponding to the camera pixel (u^c, v^c) can be solved by

$$s^p [u^p \;\; v^p \;\; 1]^t = P^p [x^w \;\; y^w \;\; z_{min} \;\; 1]^t. \tag{13}$$

Suppose projected fringe patterns vary along u^p direction on projector plane, artificial minimum phase Φ_{min} defined on camera pixel can be determined from

$$\Phi_{min}(u^c, v^c) = u^p \times 2\pi/T, \tag{14}$$

where T, again, is the number of pixels in a fringe period of the projected patterns, assuming the unwrapped phase starts from 0 radians when $u^p = 0$.

Once the minimum phase map Φ_{min} is determined, we can eliminate 2π discontinuities of the wrapped phase ϕ. Fig. 2 conceptually demonstrates the details of unwrapping process. Fig. 2(a) shows wrapped phase directly extracted from three-step phase-shifting algorithm with 2π jumps. Assume the region within the red dashed rectangle is what camera captures on the projector plane at $z^w = z_{min}$. When $z^w > z_{min}$, the region is shifted to the area shown in the solid blue window. Fig. 2(b) presents continuous phase map, where the region inside the red dashed box is the artificially generated minimum phase Φ_{min} and Fig. 2(c) plots cross sections of the unwrapped phase. With artificially created minimum phase Φ_{min}, both wrapped phases ϕ_1 and ϕ are unwrapped properly by adding 2π to the wrapped phase pixel-by-pixel if its phase value is below the corresponding point on Φ_{min}.

The same principle also applies to cases where we have more fringe periods in the captured camera image, as shown in Fig. 2(d), yet different integer fringe order $k(x, y)$ of 2π should be added to the wrapped phase ϕ depending on its difference with Φ_{min}.

$$2\pi \times (k-1) < \Phi_{min} - \phi < 2\pi \times k, \tag{15}$$

or explicitly

$$k(x, y) = ceil\left[\frac{\Phi_{min} - \phi}{2\pi}\right]. \tag{16}$$

Here, $ceil[]$ is the ceiling operator that gives the nearest upper integer number.

2.4. Depth range limitation

The geometric constraints based phase unwrapping algorithm using a single depth plane provides absolute phase maps without additional image capture, which is beneficial to high speed multiple objects measurements. In addition, ideal artificial minimum phase does not introduce extra error in fringe order calculation. However, this method has its inherent limitation on the maximum depth range that it can handle, as mentioned by An et al. [27].

Fig. 3 illustrates depth limitation of the geometric constraints based phase unwrapping approach. The red dashed box in Fig. 3(a) highlights the region in wrapped phase map when $z^w = z_{min}$. Assume at a farther plane $z^w = z_{max}$, the phase is resultantly shifted by 2π as shown in the solid blue rectangle. One can observe that phase inside of the blue box varies in the same way as the phase in red box does. In other words, we cannot tell the difference between ϕ_1 and ϕ_2. Fig. 3(b) shows the unwrapped phase map in projector space. Here Φ^1_{min} inside the red window is the minimum phase created at $z^w = z_{min}$, which can be used to unwrap ϕ_1 correctly. If we use Φ^1_{min} to unwrap ϕ_2, the resultant unwrapped phase Φ_{21} is inside of the blue dashed window. Yet obviously, correct unwrapped phase of ϕ_2 is supposed to be located at the solid blue box shown in Fig. 3(b). We plot the cross sections of all corresponding phase maps in Fig. 3(c). ϕ_1 and ϕ_2 have identical phase distributions, which produce same fringe order k by Eq. (16) if using

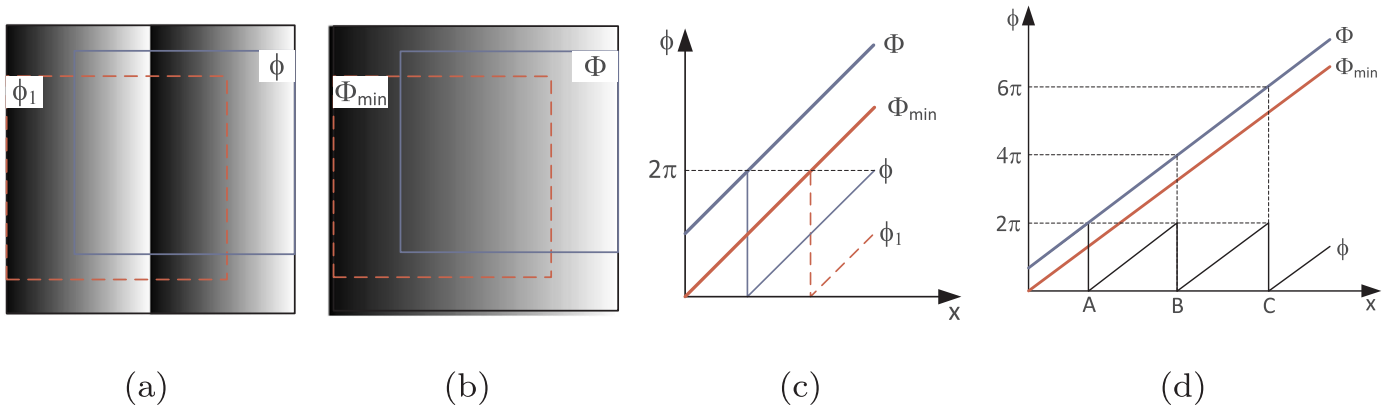

Fig. 2. Conceptual illustration on removing 2π discontinuities of wrapped phase map by solely using the minimum phase map Φ_{min} [27]. (a) Windowed regions represent the camera phase map acquired at different depths z^w: red dashed window at z_{min} and solid blue window at $z > z_{min}$; (b) Corresponding Φ_{min} and Φ defined on the projector image plane; (c) Cross sections of Φ_{min} and Φ and the wrapped phase map; (d) Example when projected fringe patterns use four periods. (For interpretation of the references to color in this figure legend, the reader is referred to the web version of this article.)

Φ^1_{min}, meaning that the corresponding unwrapped results also have same phase value. The actual unwrapped phase map Φ_{21} has a 2π shift from the correct phase map Φ^2_{min}. If z^w is further increased, the phase error could be integer k times of 2π. Therefore, geometric constraints based phase unwrapping algorithm with a single depth plane can only unwrap the phase within a depth volume ranging $[z_{min}, z_{max})$.

Fig. 4 demonstrates the geometric relationship between camera and projector light rays. The world coordinate coincides with camera lens coordinate for simplification. Point A is on z_{min} plane with absolute phase Φ_A, and point B is on the z_{max} plane. Point A and point B are imaged as the same point from camera perspective, while they have a 2π shift on phase map. Based on the analysis before, phase in point B is mistakenly unwrapped to Φ_A and corresponding 3D depth value will be calculated as z_{min}. So the length of $\overline{AB}$ is the depth range $\Delta z = z_{max} - z_{min}$ that we can properly unwrap solely by the minimum phase Φ_{min}.

Suppose the angle between camera and projector optical axis is α, and the fringe period of the projected pattern in space is T_s. From the trigonometrical derivation, we can easily calculate the maximum depth range:

$$\Delta z = T_s / \sin\alpha. \tag{17}$$

One can increase the depth range by reducing the angle α between projector and camera and/or increasing the fringe period T_s; however, changing these parameters means changes in phase quality, which is not desirable for high-accuracy measurements.

2.5. Proposed large depth range sensing method

We propose to extend the measurement range by using multiple minimum phase maps Φ_{min} created from different z^w planes. For the case in Fig. 2 as an example, we can generate another artificial phase map Φ^2_{min} at $z^w = z_{max}$ and unwrap ϕ_2 by referring to Φ^2_{min}. Both Φ^1_{min} and Φ^2_{min} can properly unwrap the phase within a Δz range. Combining Φ^1_{min} and Φ^2_{min}, the maximum depth range can be as large as $2\Delta z$. One can further extend the depth range by using more minimum phase maps for unwrapping. This section elaborates our proposed approach and how to practically implement it.

The key problem on depth range extension is how to automatically decide sections that apply different minimum phase maps. Generally speaking, we have some priori knowledge on the rough geometry of measured objects. By extracting object feature points whose relative positions are known, we can segment the object into multiple depth intervals. As long as we make sure that each depth interval is within the maximum depth range Δz, the phase in each region can be correctly unwrapped by referring to corresponding minimum phase.

A spherical object with a large depth range is used here to illustrate the basic idea of the proposed method. Fig. 5(a) is wrapped phase map from three phase-shifted fringe patterns. First we create a minimum phase map Φ^1_{min} at the closet depth plane of sphere $z^w = z_{min}$, and use this Φ_{min} to unwrap the phase map show in Fig. 5(a). Fig. 5(b) shows the unwrapped phase map, and Fig. 5(f) shows the recovered 3D geometry. The unwrapped phase map and thus 3D geometry have obvious discontinuities on the periphery of sphere where the depth value

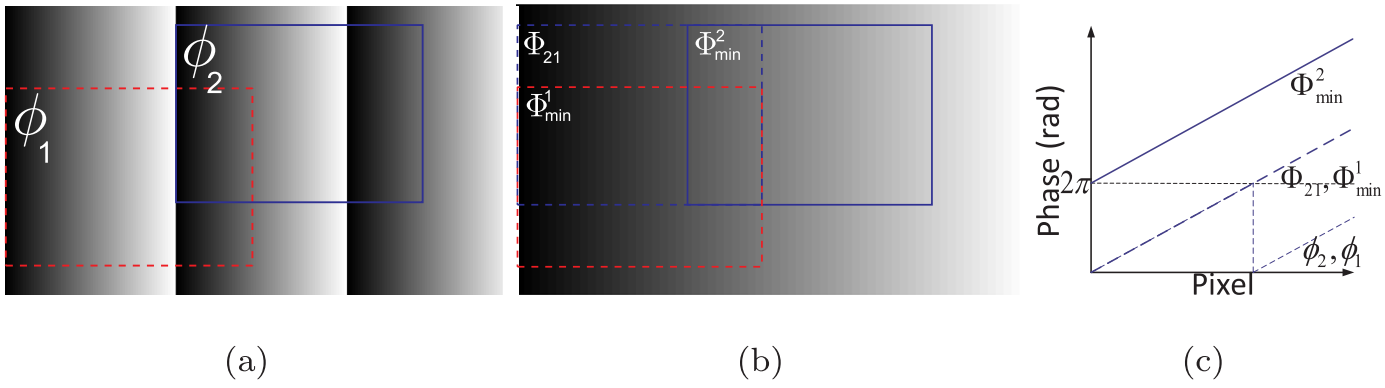

Fig. 3. Illustration of depth range limitation. (a) Windowed regions show the wrapped phase ϕ_1 and ϕ_2 acquired by the camera at different z^w depth; (b) unwrapped phase map of (a), the phase ϕ_1 is correctly unwrapped as Φ^1_{min}, yet the phase Φ_2 is unwrapped as Φ_{21} which deviates from the supposed Φ^2_{min}; (c) cross sections of corresponding phase maps in (a) and (b). (For interpretation of the references to color in this figure legend, the reader is referred to the web version of this article.)

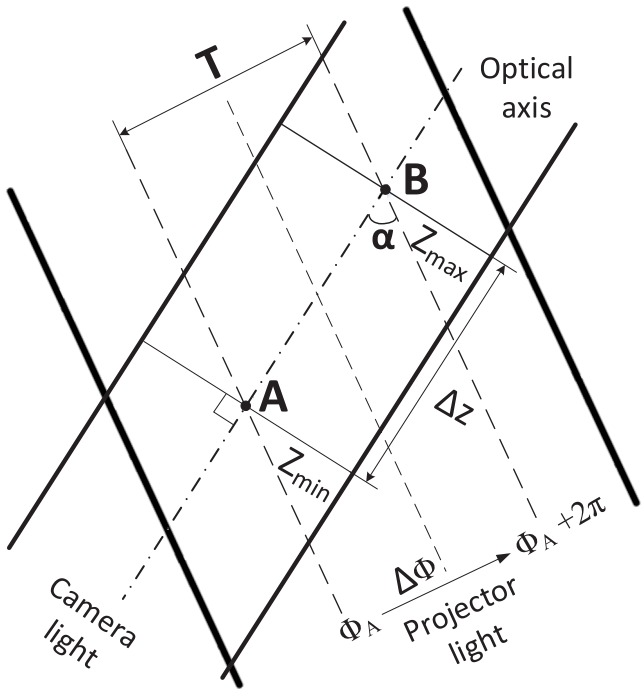

Fig. 4. A schematic diagram showing the depth limit of the phase unwrapping method using a single Φ_{min}: the point A on z_{min} plane and B on z_{max} plane are imaged the same on the camera, yet has 2π shift in absolute phase defined on the projector; the maximum depth range that can be measured without error in fringe order determination is $\Delta z = z_{max} - z_{min}$.

exceeds the maximum depth range.

We then create the second minimum phase map Φ^2_{min} at a farther z^w plane. The corresponding unwrapped phase map and 3D recovery is shown in Fig. 5(c) and (g), respectively. Apparently, the second minimum phase map cannot properly unwrap the whole range of geometry either. We then take the difference between the unwrapped phase maps from Fig. 5(b) and (c) to generate another map shown Fig. 5(d). Bright areas indicate there are differences between these two phase maps and the black areas indicate these two phase maps are the same. For the areas with same unwrapped phase, either of these two phase maps can be used for 3D reconstruction. For areas with different unwrapped phase, we utilize the rough pre-knowledge about spherical geometry to select the correct phase map: the center of the sphere is closer to the z_{min} plane; the surrounding of the sphere is farther to the z_{min} plane. So the phase map in Fig. 5(b) unwrapped from Φ^1_{min} has correct absolute phase in center part, yet the phase map in Fig. 5(b) unwrapped from Φ^2_{min} has correct absolute phase in surrounding part. The combined phase map is presented in Fig. 5(e) and corresponding 3D recovered geometry is shown in Fig. 5(h), indicating indeed the whole phase map is correctly unwrapped. By this means, the measurement depth range can be effectively extended. If object surface has larger depth range, three or more minimum phase maps can be used to further extend the measurement range, albeit the region segmentation algorithm could be more complex.

3. Experiment

To verify the performance of the proposed method, we developed a real-time 3D shape measurement system which includes a high-speed CCD camera (Model: Jai TM-6740CL) with a 16 mm focal length lens

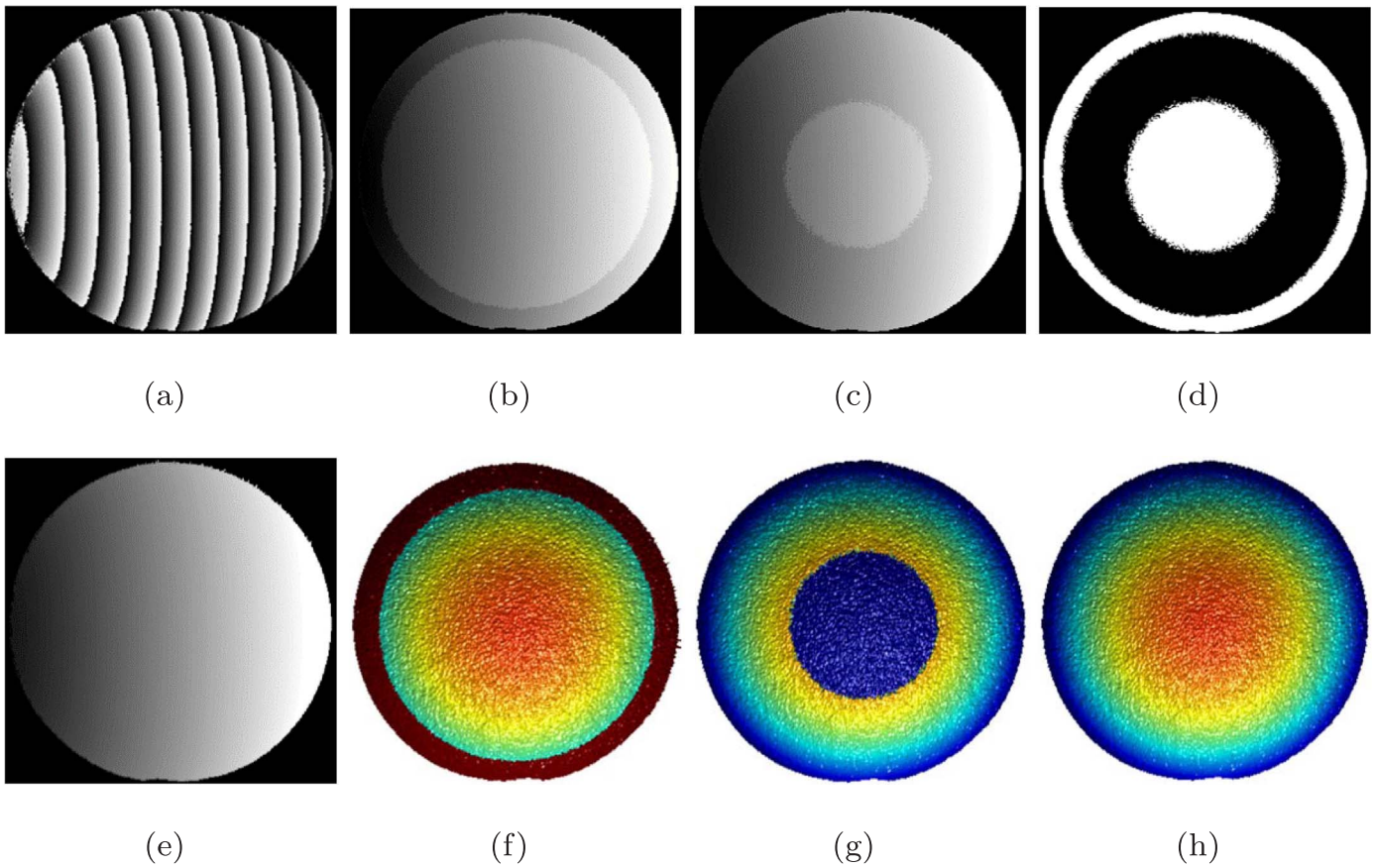

Fig. 5. An experiment showing the framework of our depth range extension method. (a) The wrapped phase map; (b) unwrapped phase map directly from a single minimum phase Φ^1_{min}; (c) unwrapped phase map from Φ^2_{min}; (d) phase map difference between (b) and (c); (e) the final unwrapped phase map combining (b) and (c); (f) 3D reconstruction for phase map shown in (c); (g) 3D reconstruction for phase map shown in (d); (h) 3D reconstruction for phase map shown in (e).

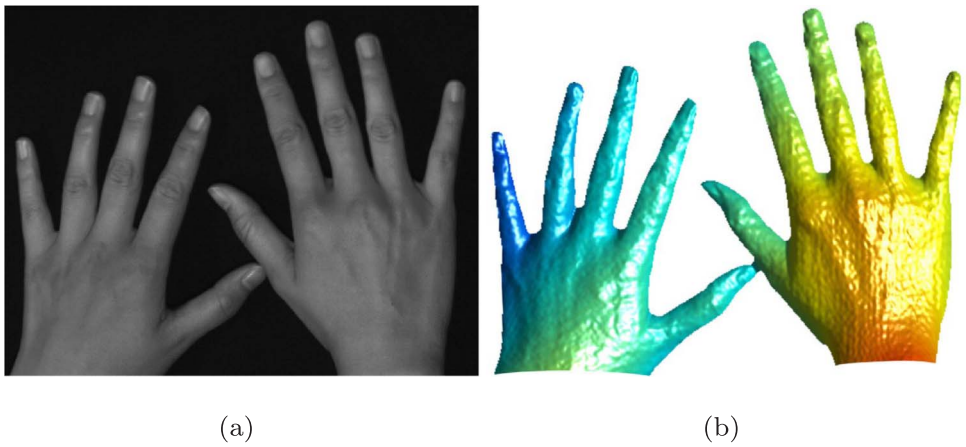

Fig. 6. One frame of a video sequence of human hands measurement in real time (associated Video 1: https://engineering.purdue.edu/ZhangLab/videos/OLE_Jiang_Video1.mp4). (a) 2D photograph; (b) 3D reconstruction.

(Model: Computer M1614-MP2) and a high-speed DLP projector (LightCrafter 4500). The camera has a resolution of 640 × 480 pixels and the lens is a 2/3-in. lens with an F/1.4 aperture. The projector's native resolution is 912 × 1140 pixels with a 31.5 mm focal length lens having an aperture of F/2.1. The system was calibrated by the method introduced by Li et al. [30] and the camera lens coordinate system was selected as the world coordinate system. For all following experiments, we chose fringe period of $T = 36$ pixels and used three equally phase-shifted fringe patterns to generate wrapped phase map.

We first performed real-time 3D shape measurement of two hands using a single minimum phase map Φ_{min}. Fig. 6 and its associated video (Video 1: https://engineering.purdue.edu/ZhangLab/videos/OLE_Jiang_Video1.mp4 illustrate the real-time measurement results. For this experiment, 2D fringe patterns were captured at 120 Hz, and thus 3D measurement speed is 40 Hz since three fringe patterns are used to recover one 3D geometry. Since the depth range of hands are pretty small (does not exceed the sensing range Δz), using a single minimum phase map Φ_{min} is sufficient to properly unwrap the phase. One may also notice that the method can measure multiple objects simultaneously. This is simply because the geometric constraint based phase unwrapping is carried out pixel by pixel without requiring any information from surrounding pixels, as discussed in Section 2.3.

Fig. 7 shows another example of measuring a large depth range statue shown in Fig. 7(a). Fig. 7(b) shows the wrapped phase from three phase-shifted fringe patterns. We generated a single minimum phase map Φ^1_{min} at $z^1_{min} = 1340$ mm, as shown in Fig. 7(c), to unwrap the wrapped phase shown in Fig. 7(b) pixel by pixel. Fig. 7(d) shows the unwrapped phase. One may notice that the phase map is not smooth. For better visualization, we reconstructed 3D geometry using this unwrapped phase map with calibration data, as shown in Fig. 7(e).

For our measurement system, the angle α between the projector optical axis and the camera optical axis is approximately 8.3° and the spatial span of one projected fringe period at $z_{min} = 1340$ mm is about $T_s = 20.32$ mm. Eq. (17) tells that the maximum depth range Δz is approximately 140.76 mm. Yet the depth range of the sculpture surface is approximately 166 mm, which exceeds the maximum depth range. Therefore, using a single minimum phase Φ_{min} cannot correctly unwrap the whole sculpture. The experimental data agrees with the numerical analysis: the reconstructed 3D geometry in Fig. 7(e) has unexpected geometric discontinuities at areas with large depth value, as shown in the two red bounding boxes.

Then we applied our proposed pre-knowledge based unwrapping algorithm to the same sculpture measurement with two minimum phase maps. For a human face like statue, our pre-knowledge is that its surface roughly agrees with convex geometry, and has obvious feature points including eyes, nose and mouth. We then extract these obvious feature points, as shown in Fig. 8(a), to identify the central facial region. Although many well-developed feature point detection algo-

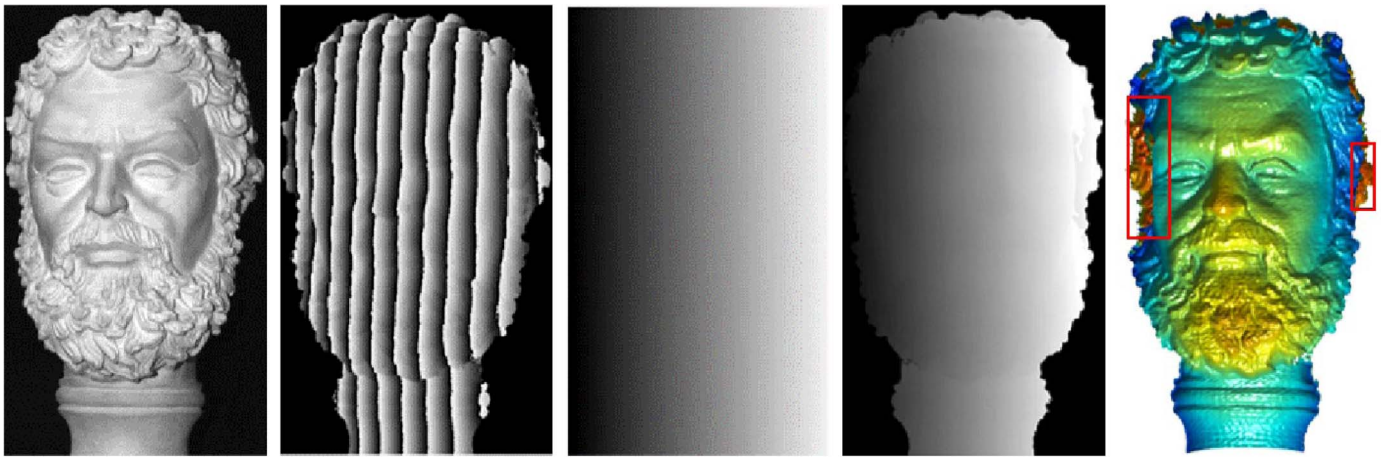

Fig. 7. Measurement of a sculpture with a single minimum phase map Φ^1_{min}. (a) A snapshot of the sculpture; (b) wrapped phase map; (c) minimum phase map Φ^1_{min}; (d) unwrapped phase map Φ^1 using minimum phase map; (e) recovered 3D geometry.

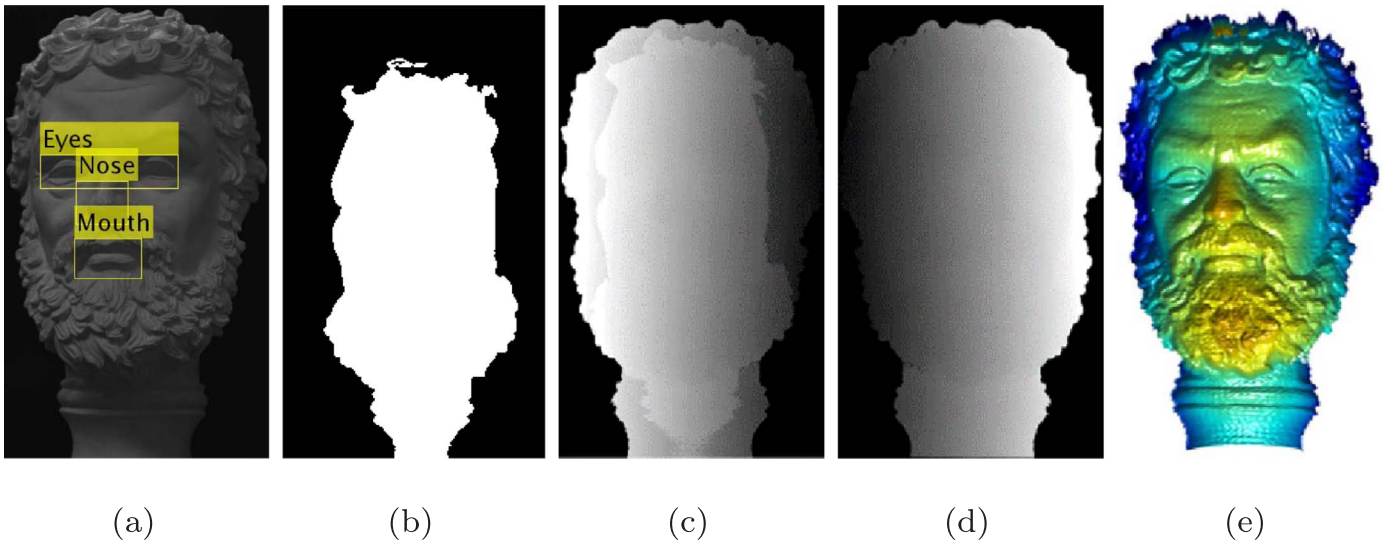

Fig. 8. Proposed absolute phase computational framework. (a) Feature detection; (b) a mask created based on the depth range containing the detected feature points; (c) unwrapped phase Φ^2 using the artificial phase map Φ^2_{min} created from maximum depth in (b); (d) absolute phase map Φ^f by merging outside the mask region from phase map shown in (c) with inside the mask region from phase map shown in Fig. 7(d); (e) reconstructed 3D geometry using the proposed framework.

rithms can be used, in this research, we adopted *vision. CascadeObjectDetector* function in Matlab Computer Vision System Toolbox to detect these feature points **F**. We started with a 3D result reconstructed from the unwrapped phase using a single Φ^2_{min}. Now we define a set of depth values Z using the depth values of feature points in Fig. 7(e)

$$Z = \{z_i(x, y) | (x, y) \in \mathbf{F}\}. \tag{18}$$

Then we created a mask **M** by

$$\mathbf{M}(x, y) = \begin{cases} 1 & \min(Z) < z(x, y) < \max(Z) \\ 0 & \text{otherwise} \end{cases}. \tag{19}$$

The mask was further refined by eliminating connected components that do not contain the feature points, and the refined mask is shown in Fig. 8(b). Next, we generated a new minimum phase Φ^2_{min} at a farther plane $z^w = \max(Z)$ to perform phase unwrapping, and the unwrapped phase in shown in Fig. 8(c). Consider we have already obtained an absolute phase map using Φ^1_{min} as shown in Fig. 7(d). Finally, we merge two absolute phase maps using the mask data shown in Fig. 8(b) to compute the final absolute phase map. Essentially, for the region outside of the mask value 0, we select the unwrapped phase Φ^2 unwrapped by Φ^2_{min}, as shown in Fig. 8(c); for the region inside of the mask value 1, we select the unwrapped phase Φ^1 unwrapped by Φ^1_{min}, as shown in Fig. 7(d), that is, the final phase is created by

$$\Phi^f(x, y) = \Phi^1(x, y) \times M(x, y) + \Phi^2(x, y) \times [1 - M(x, y)]. \tag{20}$$

The computed final absolute phase map and the recovered 3D geometry are respectively shown in Fig. 8(d) and (e), from which we can see that our proposed method can satisfactorily recover the entire 3D geometry with a large depth range.

To validate our proposed method, we measured the same statue using a temporal phase unwrapping method [17] and compared the results obtained from the single- and dual- minimum phase map methods. Fig. 9 shows the result. Fig. 9(d) shows the same cross sections of the recovered geometries. These results show that the single Φ_{min} unwrapping method (black dashed line) experiences measurement errors on the boundary where the depth value exceeds the sensing range; while the result (blue solid line) obtained from our proposed phase unwrapping method perfectly overlaps with the result (red dash dot line) from the conventional temporal phase unwrapping method, proving the success of our proposed method for large depth range absolute 3D shape measurement.

To further evaluate the accuracy of our proposed method, Fig. 10 analyzes the measurement accuracy of the proposed method by comparing the measurement results with an ideal 3D sphere with a diameter of 203.2 mm, that was used as an example in Fig. 5. Since the diameter of the measured sphere is known, we determine the position of sphere center from measured data by a least squared algorithm. After the sphere center is decided, we show the reconstructed 3D data and the ideal sphere model at the same time in Fig. 10(a). Then an error map is calculated by taking the difference between the measured data and the ideal sphere as shown in Fig. 10(b) and one cross section plot is shown in Fig. 10(c). The mean measurement error is -0.02 mm, and the standard deviation of the measurement error is approximately 0.58 mm. Clearly, the measurement accuracy of the proposed method is reasonably high.

Because of the widespread interest in facial expression capture, we measured human facial expressions. Fig. 11 and associated video (Video 2: https://engineering.purdue.edu/ZhangLab/videos/OLE_Jiang_Video2.mp4) show the result. In this experiment, a human subject shown in Fig. 11(a) was measured at 40 Hz. Fig. 11(b) shows one of the fringe patterns used to recover one 3D model, and Fig. 11(c) shows 3D reconstruction using a single Φ_{min}. Again, we use the same Matlab feature detection toolbox to detect eyes, nose and mouth for each frame to create the second Φ_{min} phase map. The same region segmentation algorithm was employed frame by frame to identify the central face area to properly select unwrapped phase regions from two unwrapped phase maps. Fig. 11(d) shows the 3D reconstruction by employing our proposed computation frame. Again, a single Φ_{min} fails to properly unwrap regions such as neck and hair, but the proposed two Φ_{min} successfully unwraps the entire image.

Since previously proposed marker-based spatial phase unwrapping method can also measure human facial expressions, the fringe patterns were embedded the same cross markers as those proposed by Zhang et al. [10]. Fig. 11(e) shows the same 3D frame recovered from the marker based method, from which one can observe that there are lots of spiky noises on the region with dark-colored hair where the fringe contrast is low and phase is noisy, failing the spatial phase unwrapping algorithm. In contrast, our 3D reconstructed data does not visually show spiky noise for those dark hair areas shown in Fig. 11(a), indicating that our proposed method is actually more robust to noise than the conventional spatial phase unwrapping algorithm. This is because conventional spatial phase unwrapping determines fringe order by referring to inherent noisy phase data surrounding that pixel, while

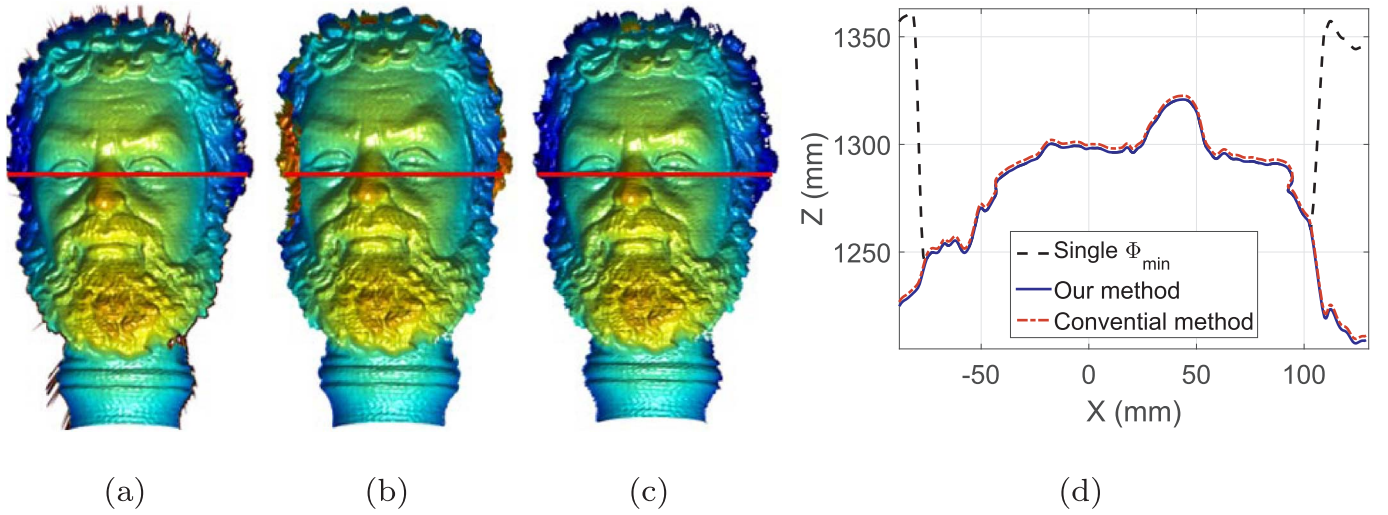

Fig. 9. Comparison between algorithms. (a) 3D result from conventional temporal phase unwrapping method; (b) 3D result from unwrapping method using a single Φ_{min}; (c) 3D result from our proposed method; (d) the same cross sections. (For interpretation of the references to color in this figure legend, the reader is referred to the web version of this article.)

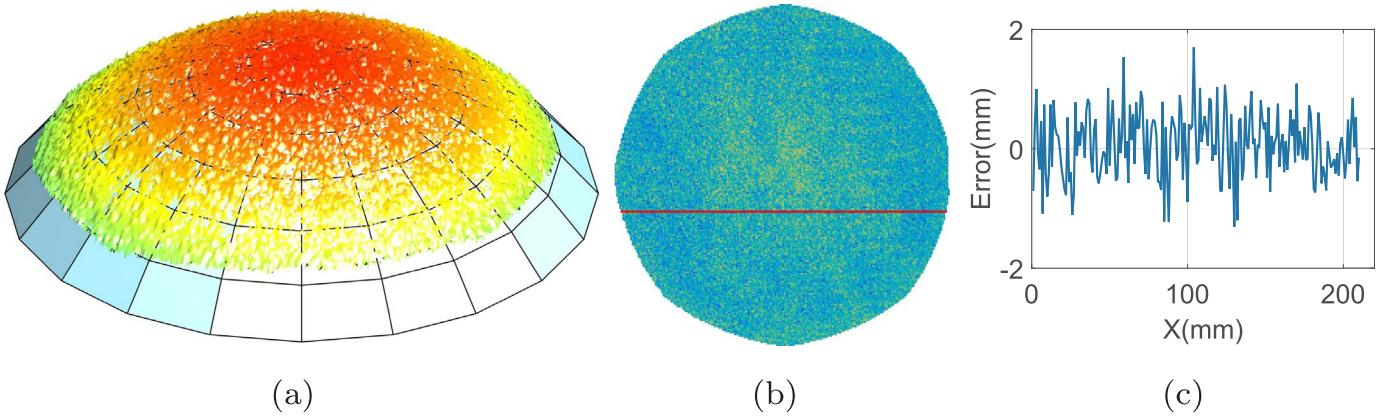

Fig. 10. The measurement error analysis by comparing with the ideal sphere with a diameter of 203.2 mm. (a) Measured sphere, shown in Fig. 5, overlays with ideal sphere; (b) Error map by taking the difference between the measured sphere and the ideal 3D sphere (mean error: −0.02 mm; standard deviation: 0.58 mm); (c) One cross section of error map shown in (b).

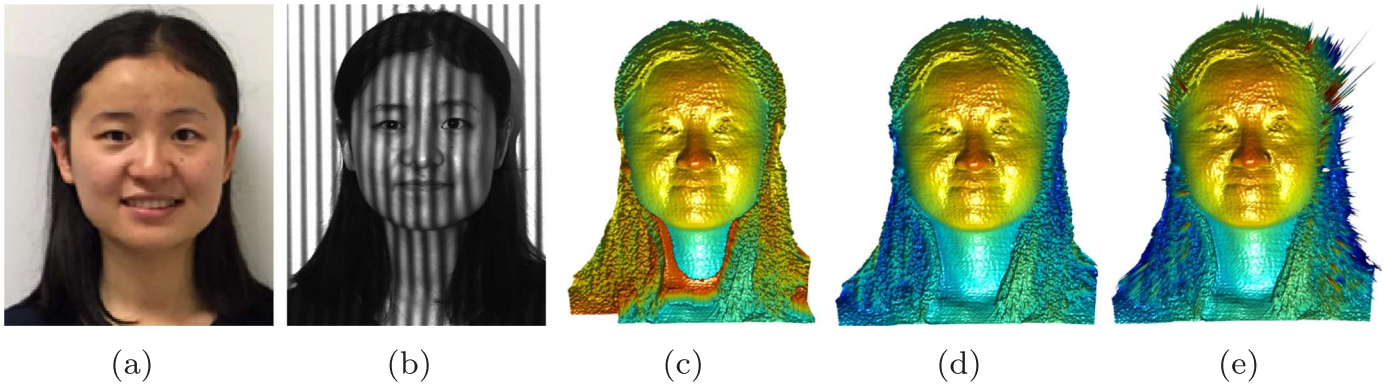

Fig. 11. Real-time 3D shape measurement of a human model (associated Video 2: https://engineering.purdue.edu/ZhangLab/videos/OLE_Jiang_Video2.mp4). (a) An actual photograph of the human model; (b) a frame of the fringe image; (c) a frame of 3D using phase unwrapping method with a single layer of Φ_{min}; (d) a frame of 3D using proposed method; (e) a frame of 3D using marker based spatial phase unwrapping approach [10].

our proposed method determines fringe order by referring to artificially created noise free phase.

Fig. 12 provides close-up views of the neck region for those 3D results shown in Fig. 11(c)–(e). Fig. 12(a)–(c) respectively shows the zoom-in rendering in 3D from single layer of Φ_{min}, the proposed method, and the spatial unwrapping method. Fig. 12(d)–(f) shows the corresponding cross section plots from Fig. 12(a)–(c). Clearly, the single Φ_{min} method fails to correctly reconstruct neck region because depth range exceeds the inherent depth limitation, as the obvious surface discontinuities shown in Fig. 12(a) and (d). Both spatial unwrapping method and the proposed method can correctly recover the same region. Fig. 13 shows the zoom-in views of the overhead region. The spatial unwrapping method fails to unwrap the low quality phase as those spiky points in hair region. But our proposed method can successfully unwrap the low-quality phase for the entire hair. These experimental data clearly show the advantage of our proposed method:

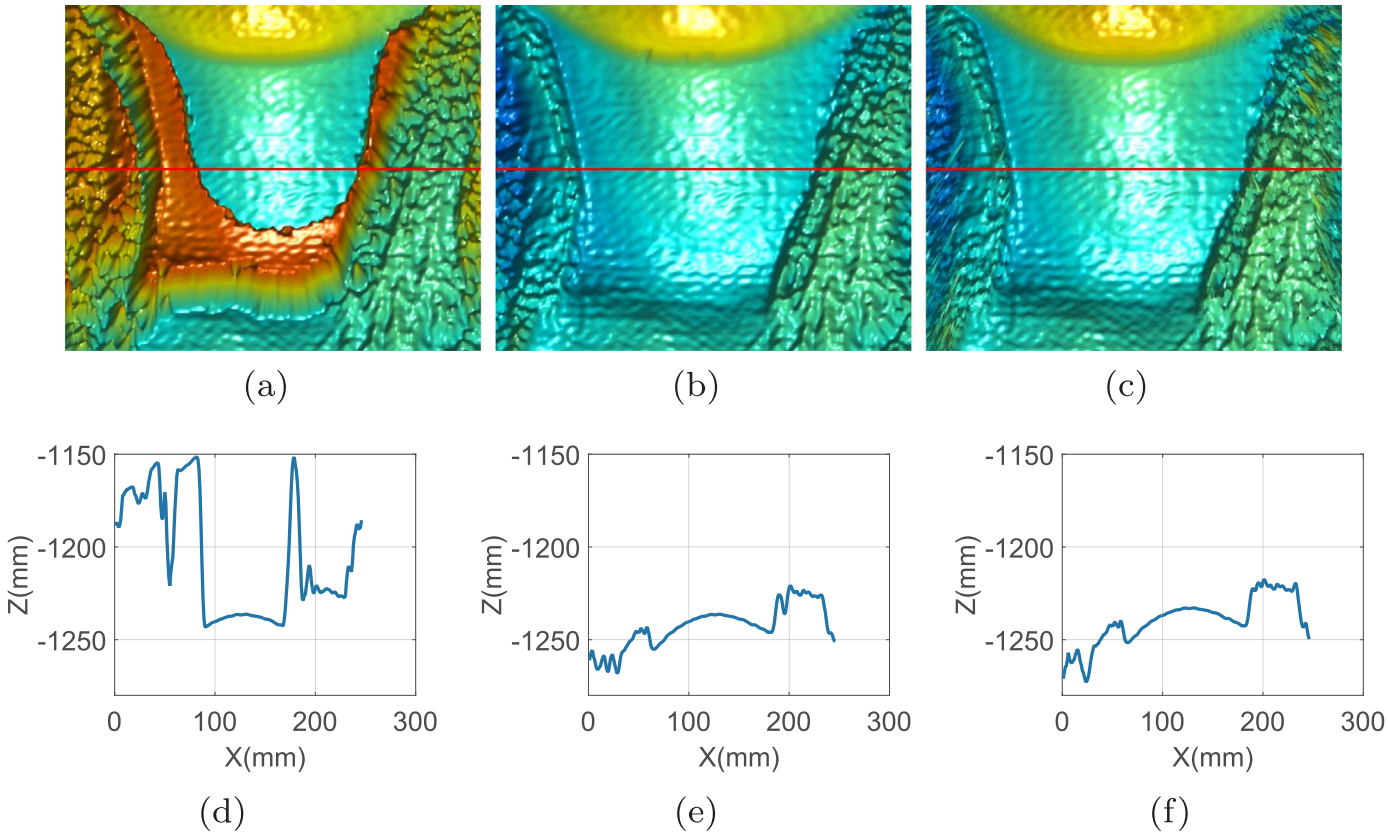

Fig. 12. Closed-up views of the neck region from Fig. 11. (a) 3D result from single Φ_{min} method; (b) 3D result from the proposed method; (c) 3D result from conventional spatial unwrapping method; (d) One cross section of (a); (e) One cross section of (b); (f) One cross section of (c).

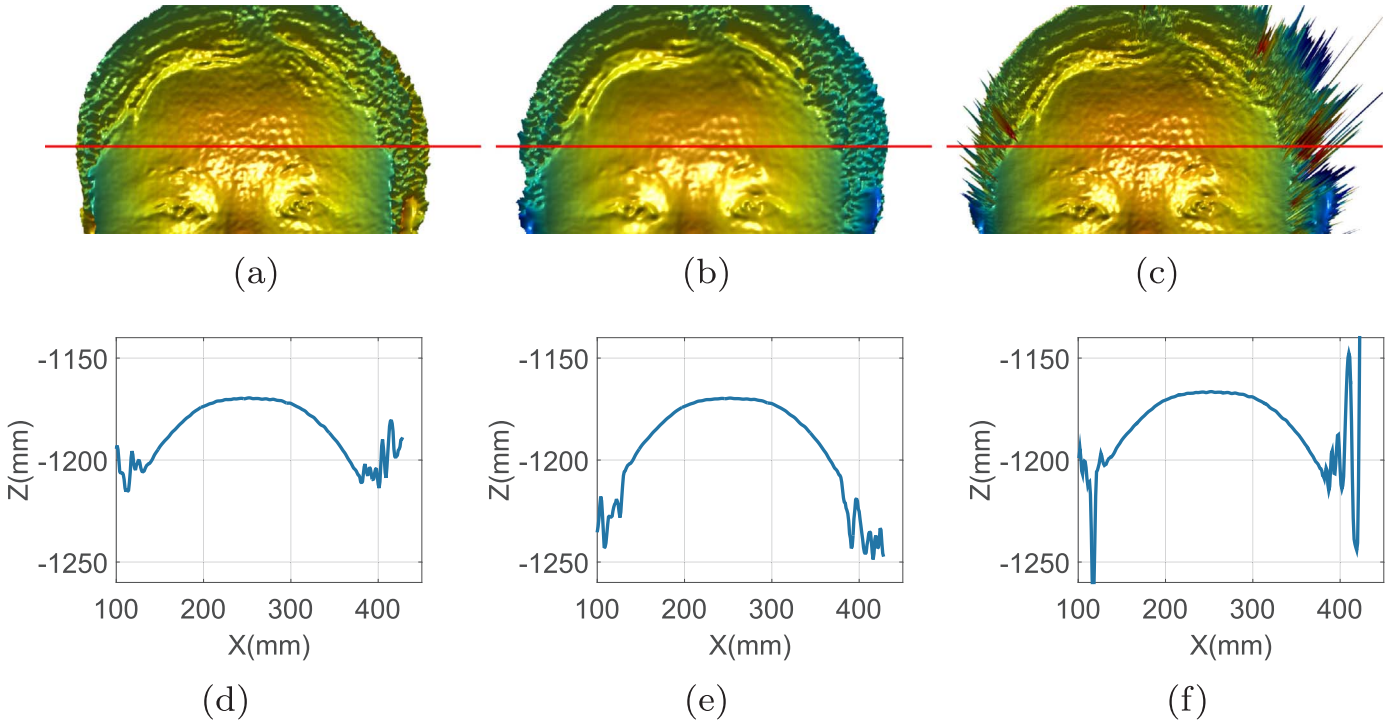

Fig. 13. Closed-up views of the overhead region from Fig. 11. (a) 3D result from single Φ_{min} method; (b) 3D result from the proposed method; (c) 3D result from conventional spatial unwrapping method; (d) One cross section of (a); (e) One cross section of (b); (f) One cross section of (c).

can handle larger depth range than the single Φ_{min} method, and can successfully unwrap low quality phase that fails the conventional spatial phase unwrapping algorithm.

4. Summary

This paper has presented a novel absolute phase computational framework that only requires three phase-shifted fringe patterns to

perform pixel by pixel absolute 3D shape measurement with a large depth range without embedding any markers, capturing additional images, or introducing additional hardware. The proposed method uses rough priori knowledge of the measured object geometry and the features on the object to segment the objects into different depth regions, and then use different artificial phase maps, generated through geometric constraints of the DFP system, to unwrap phase pixel by pixel. By this means, the proposed method substantially extends the depth range of the geometric constraint phase unwrapping method that An et al. [27] developed previously. Experiment data successfully demonstrated the effectiveness of our proposed method. Since only three fringe patterns are required, the proposed phase unwrapping method can also perform high-speed 3D shape measurement. We have developed a single-camera, single-projector 3D shape measurement system that can perform absolute 3D measurement pixel by pixel at 40 Hz.

Acknowledgments

We would like to thank the team members in our lab at Purdue University for their previous development and valuable discussions.

This work was partially sponsored by the start up funds for Prof. Song Zhang provided by Purdue University.

References

[1] Takeda M, Mutoh K. Fourier transform profilometry for the automatic measurement of 3-d object shapes. Appl Opt 1983;22:3977–82.
[2] Kemao Q. Windowed fourier transform for fringe pattern analysis. Appl Opt 2004;43:2695–702.
[3] Kemao Q. Two-dimensional windowed fourier transform for fringe pattern analysis: principles, applications and implementations. Opt Laser Eng 2007;45:304–17.
[4] Malacara D. (Ed.), Optical shop testing, 3rd Edition. New York, NY: John Wiley and Sons; 2007.
[5] Ghiglia DC, Pritt MD. (Eds.), Two-dimensional phase unwrapping: theory, algorithms, and software. New York: John Wiley and Sons; 1998.
[6] Su X, Chen W. Reliability-guided phase unwrapping algorithm: a review. Opt Laser Eng 2004;42(3):245–61.
[7] Guo H, Huang PS. Absolute phase technique for the fourier transform method. Opt Eng 2009;48(4):043609.
[8] Xiao Y, Su X, Zhang Q, Li Z. 3-d profilometry for the impact process with marked fringes tracking. Opto-Electron Eng 2007;34(8):46–52.
[9] Budianto B, Lun P, Hsung T-C. Marker encoded fringe projection profilometry for efficient 3d model acquisition. Appl Opt 2014;53(31):7442–53.
[10] Zhang S, Yau S-T. High-resolution, real-time 3-d absolute coordinate measurement based on a phase-shifting method. Opt Express 2006;14(7):2644–9.
[11] Gai S, Da F. A novel phase-shifting method based on strip marker. Opt Lasers Eng 2010;48(2):205–11.
[12] Cui H, Liao W, Dai N, Cheng X. A flexible phase-shifting method with absolute phase marker retrieval. Measurement 2012;45(1):101–8.
[13] Cheng Y-Y, Wyant JC. Two-wavelength phase shifting interferometry. Appl Opt 1984;23:4539–43.
[14] Cheng Y-Y, Wyant JC. Multiple-wavelength phase shifting interferometry. Appl Opt 1985;24:804–7.
[15] Towers DP, Jones JDC, Towers CE. Optimum frequency selection in multi-frequency interferometry. Opt Lett 2003;28:1–3.
[16] Wang Y, Zhang S. Superfast multifrequency phase-shifting technique with optimal pulse width modulation. Opt Express 2011;19(6):5143–8.
[17] Sansoni G, Carocci M, Rodella R. Three-dimensional vision based on a combination of gray-code and phase-shift light projection: analysis and compensation of the systematic errors. Appl Opt 1999;38:6565–73.
[18] Zhang S. Flexible 3d shape measurement using projector defocusing: extended measurement range. Opt Lett 2010;35(7):931–3.
[19] Wang Y, Zhang S. Novel phase coding method for absolute phase retrieval. Opt Lett 2012;37(11):2067–9.
[20] Zuo C, Chen Q, Gu G, Feng S, Feng F, Li R, Shen G. High-speed three-dimensional shape measurement for dynamic scenes using bi-frequency tripolar pulse-width-modulation fringe projection. Opt Lasers Eng 2013;51(8):953–60.
[21] Xing Y, Quan C, Tay C. A modified phase-coding method for absolute phase retrieval. Opt Lasers Eng (in press).
[22] Zhong K, Li Z, Shi Y, Wang C, Lei Y. Fast phase measurement profilometry for arbitrary shape objects without phase unwrapping. Opt Lasers Eng 2013;51(11):1213–22.
[23] Li Z, Zhong K, Li YF, Zhou X, Shi Y. Multiview phase shifting: a full-resolution and high-speed 3d measurement framework for arbitrary shape dynamic objects. Opt Lett 2013;38(9):1389–91.
[24] Bräuer-Burchardt C, Kühmstedt P, Notni G. Code minimization for fringe projection based 3d stereo sensors by calibration improvement. Technical report, arXiv:1404.7298
[25] Song K, Hu S, Wen X, Yan Y. Fast 3d shape measurement using fourier transform profilometry without phase unwrapping. Opt Lasers Eng 2016;84:74–81.
[26] Lohry W, Chen V, Zhang S. Absolute three-dimensional shape measurement using coded fringe patterns without phase unwrapping or projector calibration. Opt Express 2014;22(2):1287–301.
[27] An Y, Hyun J-S, Zhang S. Pixel-wise absolute phase unwrapping using geometric constraints of structured light system. Opt Express 2016;24(16):18445–59.
[28] Zhang Z. A flexible new technique for camera calibration. IEEE Trans Pattern Anal Mach Intell 2000;22(11):1330–4.
[29] Zhang S, Huang PS. Novel method for structured light system calibration. Opt Eng 2006;45(8):083601.
[30] Li B, Karpinsky N, Zhang S. Novel calibration method for structured light system with an out-of-focus projector. Appl Opt 2014;53(16):3415–26.